

# Audiogram Digitization Tool for Audiological Reports

François Charih  
Systems and Computer Engineering  
Carleton University  
Ottawa, ON, Canada  
francoischarih@sce.carleton.ca

James R. Green  
Systems and Computer Engineering  
Carleton University  
Ottawa, ON, Canada  
jrgreen@sce.carleton.ca

**Abstract**—A number of private and public insurers compensate workers whose hearing loss can be directly attributed to excessive exposure to noise in the workplace. The claim assessment process is typically lengthy and requires significant effort from human adjudicators who must interpret hand-recorded audiograms, often sent via fax or equivalent. In this work, we present a solution developed in partnership with the Workplace Safety Insurance Board of Ontario to streamline the adjudication process. In particular, we present the first audiogram digitization algorithm capable of automatically extracting the hearing thresholds from a scanned or faxed audiology report as a proof-of-concept. The algorithm extracts most thresholds within 5 dB accuracy, allowing to substantially lessen the time required to convert an audiogram into digital format in a semi-supervised fashion, and is a first step towards the automation of the adjudication process. The source code for the digitization algorithm and a desktop-based implementation of our NIHL annotation portal is publicly available on GitHub <https://github.com/GreenCUBIC/AudiogramDigitization>.

**Index Terms**—audiology, transfer learning, digitization, noise-induced hearing loss

## I. INTRODUCTION

Noise-induced hearing loss (NIHL) is a common consequence of long term exposure to noise in the workplace. In fact, a Canadian study [1] recently found, through a series of over 3,500 interviews, that 42% of respondents were exposed to hazardous levels of noise in the workplace. Moreover, 20% of respondents who reported being asked to wear hearing protective equipment by their employer admitted to not following this rule consistently. It is therefore not surprising that a large number of occupational NIHL claims are received by public and private insurance companies yearly.

The Workplace Safety Insurance Board of Ontario (WSIB) reports receiving several thousands of NIHL-related claims every year which can take several months to process. The audiological reports received must be carefully interpreted by adjudicators who apply a series of rules to determine the eligibility of the claim. This is a time consuming process that contributes to the lengthy adjudication process.

The audiogram is a critical component of a NIHL-related claim. An audiogram plots the hearing *threshold* (minimal perceivable amplitude) in dB across a range of frequencies.

This project would not have been possible without the financial support provided by the Workplace Safety Insurance Board of Ontario.

Different standard audiological symbols are used to indicate the whether a hearing thresholds correspond to the left or right ear, whether the threshold was obtained through air or bone conduction, and whether masking was used or not to prevent the non-test hear from hearing tones delivered to the other ear. The shape of this audiometric curve is pivotal in establishing the etiology of the hearing loss. For instance, individuals with NIHL tend to have a notch in their air and bone conduction audiometric curves (worse hearing) between 3,000 and 6,000 Hz [2].

While audiometers are now fully capable of generating digital versions of audiograms, many hearing hearing professionals still plot audiograms by hand in audiological reports. While these reports differ slightly in their layout and content, they typically consist of a single page with one or two audiogram plots (combined or separated by ear), a brief summary of the findings, and potentially results from other tests (eg. tympanogram, *etc.*).

Because the reports are received by fax or as image files sent electronically, eligibility rules can only very rarely be directly applied to reports submitted to insurance companies or compensation boards. As such, an algorithm capable of automatically extracting hearing thresholds from the audiograms on scanned or faxed audiological records to add to the client's electronic record could significantly reduce the time required to process a claim.

To the best of our knowledge, there exists no publicly available audiogram digitizer capable of extracting thresholds from scanned or faxed audiological reports. In this work, completed in partnership with the WSIB, we present an audiogram digitization algorithm combining traditional image processing and deep neural networks trained with transfer learning to digitize audiograms. We outline how the training data for this algorithm were collected, the training procedure, and show how the algorithm can be useful in the adjudication of NIHL-related claims.

## II. DIGITIZATION STRATEGY

In order to extract hearing thresholds from an audiological report, the following elements (shown in Figure 1) must be located and identified:

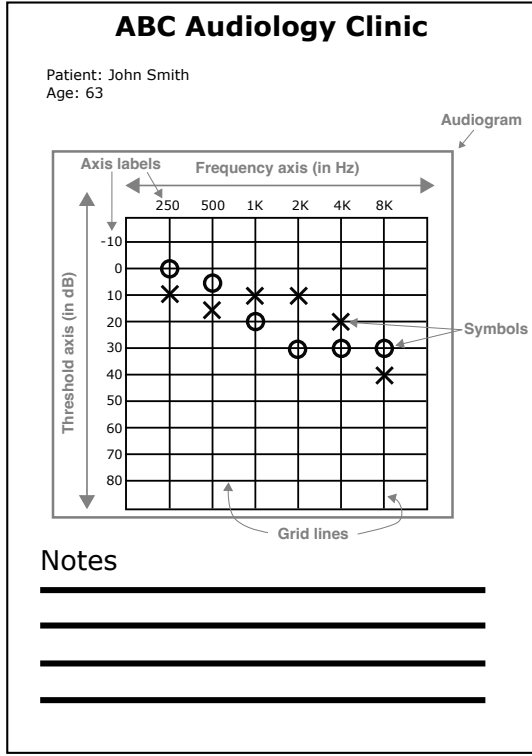


Fig. 1. **Components of interest within a typical audiology report.** A typical audiology report contains general information about the patient, the audiogram, and a section for notes. Occasionally, the report will also contain tympanometry data in tabular or graphical form. The elements of interest that are extracted for the purpose of this work are identified in gray.

- 1) **Audiogram:** to identify the region(s) of interest in the report.
- 2) **Axis labels and grid lines:** important for the conversion of pixel coordinates to frequency-threshold coordinates.
- 3) **Audiological symbols:** the hearing thresholds of the individual.

A number of techniques were considered to tackle the object detection problem. For instance, we initially considered applying template matching to locate the audiological symbols within the report, but rapidly realized that a number of problems made this approach less than ideal. First, the symbols are often drawn by hand, and a given symbol (e.g., a cross) will be drawn differently depending on the person recording the audiogram. Next, overlapping symbols are a frequent occurrence, and as such, it is not uncommon to see 2 or 3 overlapping symbols. For these reasons, the number of templates that would be required to handle all possible symbols and symbol combinations would be prohibitively large.

We finally settled for the strategy illustrated in Figure 2. This strategy combines transfer learning (object detection) and traditional image processing techniques. Pre-trained deep convolutional neural networks are fine-tuned for detection of audiograms, axis labels, and symbols within a report. Line detection techniques are applied to correct for audiogram rotation

and to compute the pixel-to-frequency/threshold transform. The algorithm is described in greater details later in this paper.

### III. DATA COLLECTION

Knowing that transfer learning would be employed to train object detectors for elements composing the audiological report, we sought to assemble a dataset of several thousands of annotated audiological reports.

The WSIB provided a large dataset of approximately 3,200 anonymized audiological reports from claims received in 2006 or later. The reports all consisted of a single page on which the audiograms were drawn using one or two plots. A qualitative assessment of the dataset revealed a highly heterogeneous dataset where reports varied greatly in terms of layout, resolution, handwriting, and completeness.

To collect the annotations required to develop and evaluate the strategy presented previously, we developed the *NIHL Portal*, a web portal specifically tailored to collect the required data rapidly and ergonomically. The user interface was developed using React.js (<https://reactjs.org>) while its backend was implemented using Flask (<https://flask.palletsprojects.com>) as the server and PostgreSQL (<https://www.postgresql.org/>) as the database.

Annotators were asked to draw, using the interface shown in Figure 4, bounding boxes for the audiogram, the axis labels, and the individual threshold symbols. Annotators were also asked to indicate the location of the audiogram corners along with the corresponding frequency/threshold coordinates, so that a ground truth audiogram could be computed from the annotation. The annotation process was completed over a period of approximately 4 months. The JSON schema of the annotations collected is presented in Figure 3.

### IV. DIGITIZATION ALGORITHM

#### A. Audiogram Detection Model and Rotation Correction

We used the YOLOv5s architecture developed by Ultralytics [3] pre-trained on the COCO dataset [4] to train an audiogram detection model. The main purpose of this component of the digitization algorithm is to isolate the audiogram(s) in the report so as to 1) determine whether there are audiograms in the report and 2) prevent the detection of symbols that are outside the bounds of an audiogram plot.

The audiogram detection model was fine-tuned as per the instructions described by the architecture's authors [3] on a computer with a NVIDIA P100 GPU and 64G RAM. We used 80% of the 3,000 reports for training, while the remaining 20% was used for validation. We set 206 reports aside for testing. The model was trained for 50 epochs and we selected the model that had the lowest generalized intersection over union (GIoU) [5] in validation.

When deployed, this model is used to crop the image of a report around the audiogram(s). It is often the case that the orientation of the audiogram plot must be corrected so as to make its grid lines horizontal and vertical. To this end, we framed the problem of rotation correction as an optimization one.

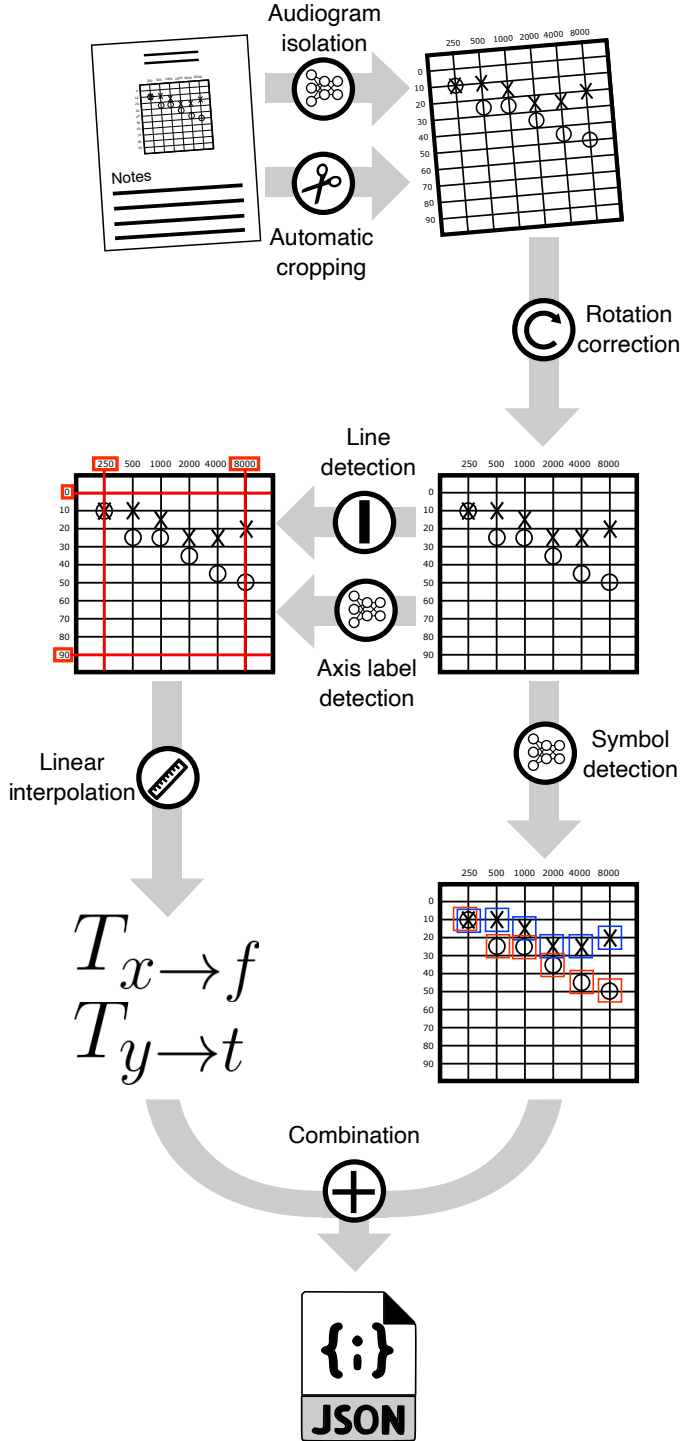


Fig. 2. **Audiogram digitization strategy.** Our strategy combines a series of deep learning-based object detection tasks with traditional image processing procedures (line detection, cropping, rotation). These steps enable the derivation of pixel-to-frequency and pixel-to-threshold transforms through linear interpolation. These transforms are subsequently applied to the pixel coordinates of detected audiological symbols to generate a JSON document listing the individual hearing thresholds.

```
[
  {
    "boundingBox": {
      "x": number,
      "y": number,
      "width": number,
      "height": number
    },
    "corners": [
      {
        "x": number,
        "y": number,
        "position": {
          "vertical": string,
          "horizontal": string
        },
        "frequency": number,
        "threshold": number,
      }, ...
    ],
    "labels": [
      {
        "boundingBox": {
          "x": number,
          "y": number,
          "width": number,
          "height": number
        },
        "value": string
      }, ...
    ],
    "symbols": [
      {
        "boundingBox": {
          "x": number,
          "y": number,
          "width": number,
          "height": number
        },
        "response": boolean,
        "measurementType": string
      }, ...
    ]
  }, ...
]
```

Fig. 3. **Schema of a JSON annotation produced by the NIHL Portal.** Annotations are stored as an array of one or two items, one for each audiogram in the report. The locations of the audiogram bounding box, corners of the audiogram, axis labels, and symbols are collected.

The first step of the procedure involves detecting lines in the audiogram with the conventional Hough Transform [6]. Lines that do not intersect another line roughly perpendicularly ( $\pm 1^\circ$ ) are not considered by the algorithm, as they are unlikely to belong to the audiogram grid. The correction angle,  $\theta_{corr}$ , is then obtained by minimizing the sum of the deviations of all lines from the horizontal ( $0^\circ$ ) or vertical axis ( $90^\circ$ ), whichever is closest in terms of angle:

$$\operatorname{argmin}_{\theta_{corr}} \left( \sum_{v \in V} |90^\circ - (\theta_v + \theta_{corr})| + \sum_{h \in H} |(\theta_h + \theta_{corr})| \right) \quad (1)$$

where  $V$  is the set of lines assumed to be vertical in the

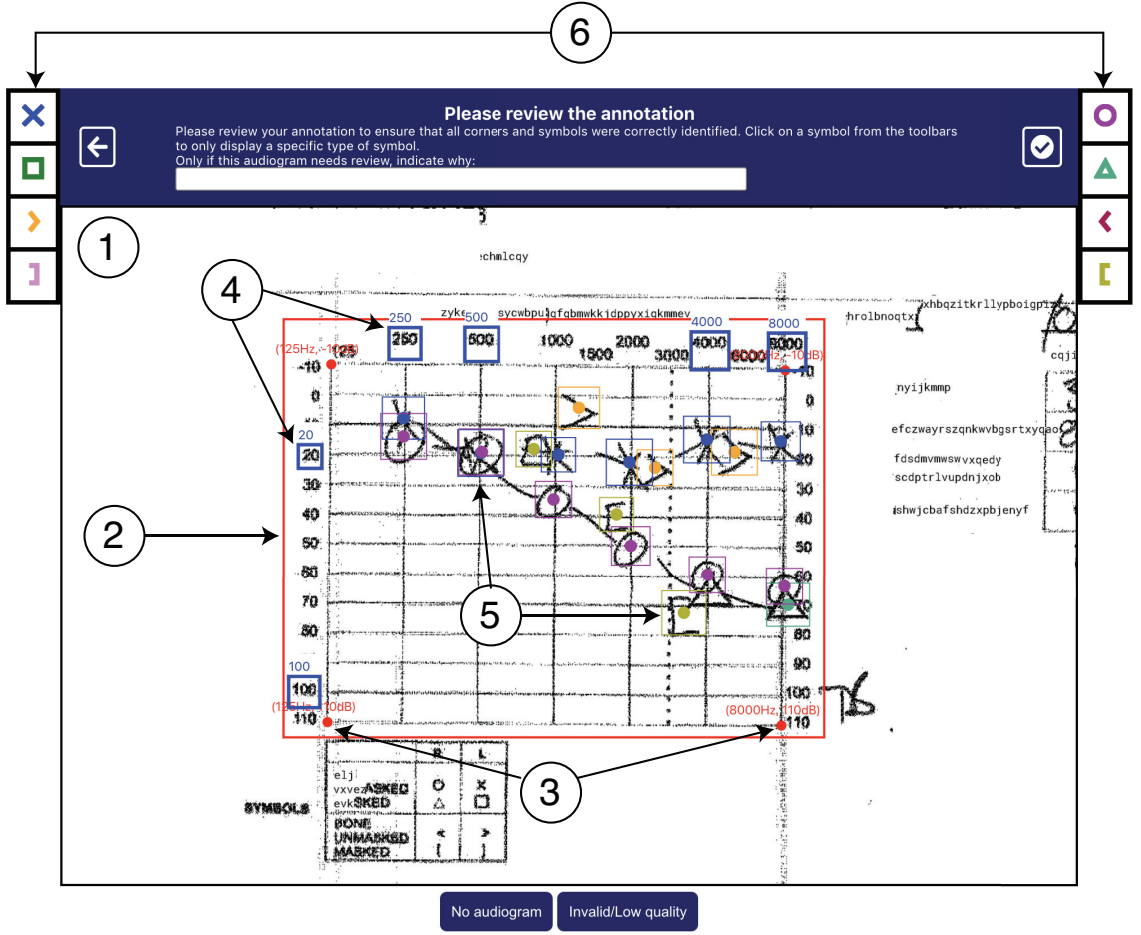


Fig. 4. **NIHL Portal**. The annotator is shown the image of an audiological report in the viewport (1) and is asked to draw the bounding box around the audiogram (2). The annotator then proceeds to annotate the outermost corners (3), the axis labels (4), and the audiological symbols (5) by selecting the appropriate symbols from a tool bar (6).

actual, unaltered report, i.e.  $\theta_v \in (45^\circ, 135^\circ)$ , and  $H$  is the set of all other lines, assumed to be horizontal in the original, unaltered report, i.e.  $\theta_h \in (-45^\circ, 45^\circ)$ .

### B. Audiological Symbol Detection

The audiological symbol detection model was trained similarly, on the same 3,000 annotated reports. We defined a total of 8 different classes corresponding to different audiological symbols accounting for the 4 different types of measurement (Table I).

TABLE I  
RELEVANT AUDIOLOGICAL SYMBOLS CONSIDERED IN THIS STUDY

	Measurement type		Ear	
	Conduction	Masking	Left	Right
1	Air	No	×	○
2	Air	Yes	□	△
3	Bone	No	>	<
4	Bone	Yes	]	[

Once trained, the model can detect the symbols and provide the pixel coordinates of the center of any detected symbol's

bounding box. However, to be clinically meaningful, these pixel coordinates must be converted into frequency-threshold pairs.

### C. Axis Label Detection

Given that the audiogram grids vary slightly in layout from one report to another, we sought to identify the axis labels so that they could be associated to the lines that make up the audiogram grid. This association allows for the derivation of pixel-to-frequency and pixel-to-threshold mappings. The derivation of these transforms using linear interpolation requires a minimum of two correct grid-line associations per axis. Ideally, these grid-line associations are at the opposite ends of the axes.

We initially attempted to apply optical character recognition to detect axis labels using Google's open-source Tesseract engine [7], but failed to obtain reliable results despite our best efforts to preprocess the images by adjusting parameters such as the contrast and brightness or by applying techniques like thresholding and dilation/erosion. However, given that the set of labels encountered is finite, we framed this as an object detection problem to be solved in the same way as audiogram

detection, and collected axis label annotations for 506 reports, and used 465 for training/validation and 41 for testing.

We fine-tuned the same YOLOv5s model on a dataset of audiograms with annotations for the following frequency axis labels: 250 Hz, 500 Hz, 4,000 Hz and 8,000 Hz. We also included classes for equivalent representations of the same frequencies (e.g. “0.25”, “0.5”, “4K”, “8”, *etc.*). The classes for the decibel axis labels included “20”, “60”, “80” and “100”. We replicated the procedure described in the previous section to train the axis label detection model.

#### D. Deriving and Applying the Pixel Domain-to-Audiological Domain Transforms

While it is trivial for human interpreters to identify the coordinates of thresholds in the *audiological domain* (in terms of frequencies and threshold values) by visual inspection of the symbol and the surrounding axes, this task is far from trivial for computers which operate in the *pixel domain*. One could presume that given enough annotated audiograms, deep neural networks could be trained to extract this information from images of audiograms. However, given the wide variety of audiograms one may encounter, all unique in terms of their layout, font, size, aspect ratio, it is highly unlikely that a couple thousands of audiogram would suffice.

Fortunately, one can make use of visual landmarks in the audiogram to derive the transforms that convert pixel values along the  $x$  axis to frequencies (in Hz) and pixel values along the  $y$  axis as thresholds (in dB). The most relevant landmarks are the axis labels and the audiogram grid lines. *Isn't that how we, humans, interpret this type of visual information after all?*

To derive the pixel-to-threshold transform (i.e. the  $y$  axis), we pair detected axis labels with the horizontal line ( $\pm 1^\circ$ ) that intersects it and that is closest to the center of its bounding box. The lines are detected with the Hough transform [6]. From this, we may generate a sorted list of tuples of the form

$$\{(y_1, t_1), \dots, (y_n, t_n)\} \quad (2)$$

where  $y_i$  is the  $y$  coordinate (in pixels) of the  $i$ -th horizontal line and  $t_i$  is the threshold value (in dB) of the associated label.

Provided that we are able to make two such associations, a transform can be derived. If more than two such associations exist, the ones that are farthest apart are used for increased resolution. The transform  $T_{y \rightarrow t}$  is simply:

$$T_{y \rightarrow t}(y) = t_1 + \frac{(t_n - t_1)(y - y_1)}{y_n - y_1} \quad (3)$$

We may proceed similarly for the pixel-to-frequency transform along the  $x$  axis, except that one must account for the logarithmic nature of the frequency scale. To do so, we use the linear *octave scale*, where 125 Hz is the  $0^{th}$  octave, 250 Hz is the  $1^{st}$  octave, 500 Hz is the  $3^{rd}$  octave, and so on. We can convert the frequency to its octave value with the equation:

$$o(f) = \frac{\ln(f/125)}{\ln(2)} \quad (4)$$

```
[
  {
    "frequency": number, // in Hz
    "threshold": number, // in dB
    "masking": bool,
    "ear": string, // "left" or "right"
    "conduction": string // "air" or "bone"
  }, ...
]
```

Fig. 5. **JSON schema of a digitized audiogram.** The JSON document produced by the algorithm is a list of JSON objects that describe the threshold of hearing, which ear was tested, the measurement type (air or bone) as well as whether masking was used or not for each frequency tested.

where  $f$  is the frequency and  $o(f)$  is the octave value of frequency  $f$ .

Then proceeding in a similar fashion as for the pixel-to-threshold transform derivation, we may generate a sorted list of tuples by associating  $x$  axis labels with the vertical lines ( $\pm 1^\circ$ ):

$$\{(x_1, o_1), \dots, (x_n, o_n)\} \quad (5)$$

where  $x_i$  is the  $x$  coordinate (in pixels) of the  $i$ -th horizontal line and  $t_i$  is the octave value of the associated frequency label.

Then, we may use linear interpolation to derive the pixel-to-frequency transform  $T_{x \rightarrow f}$ , which converts back the octave value generated into a frequency value by applying the reciprocal of Equation 4:

$$T_{x \rightarrow f}(x) = 125 \times 2^{o_1 + \frac{(o_n - o_1)(x - x_1)}{x_n - x_1}} \quad (6)$$

The frequency-threshold pairs generated by applying these transforms to the coordinates of detected symbols virtually always yield values that approximate the clinical measurements. Knowing that thresholds are measured at a set of standard octave or semi-octave frequencies and that thresholds are measured in increment of 5, we may correct the measurement by “snapping” the frequency value to the nearest standard octave or semi-octave and the threshold value to the nearest increment of 5. For instance, an initial measurement of 53.3 dB at 1,136 Hz would be corrected to 55 dB at 1,000 Hz. The rounded measurements can then be used to populate a list of thresholds in JSON format (Figure 5).

## V. RESULTS AND DISCUSSION

### A. Performance of Individual Report Component Detectors

To evaluate each independent object detector, we applied the audiogram and symbol models to the 206 reports set aside during training, and applied the axis label model to 40 reports that were held out during training. We computed the mean recall, mean precision and mean average precision at 0.5 IoU (mAP@0.5) for each model. The metrics are averaged over the different classes for the axis label and symbol models (Table II).

Unsurprisingly, the easiest task is that of detecting audiograms within an audiology report. The model trained to do so



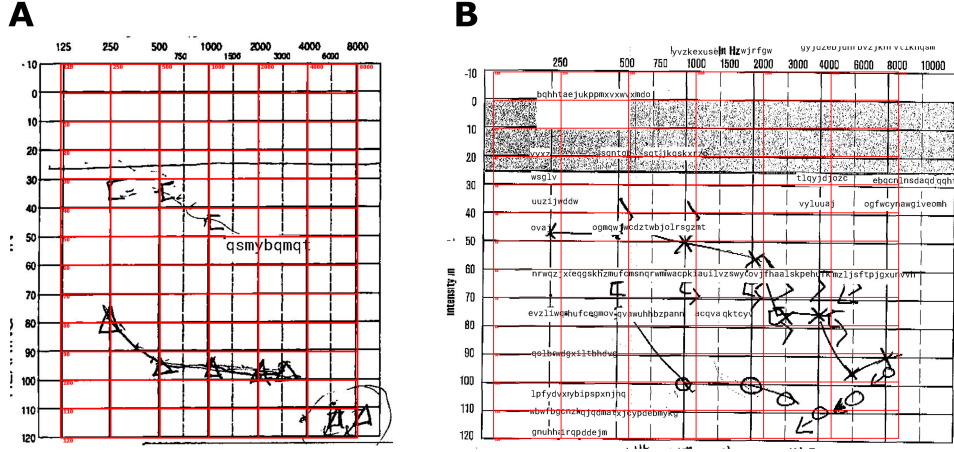


Fig. 6. **Grid reconstruction from derived transforms.** The grid derived from the transforms are shown for an instance where the grid extraction was accurate and inaccurate. In (A), the frequency and threshold lines of the extracted grid align almost perfectly with those from the report. In (B), the grid extraction portion of the algorithm failed to derive an appropriate pixel-to-frequency transform because false vertical lines were detected in the fuzzy region between 0 and 25 dB.

TABLE II  
PERFORMANCE OF THE INDIVIDUAL OBJECT DETECTION MODELS ON 200  
UNSEEN REPORTS

	Model		
	Audiogram	Axis Label	Symbol
Recall	1.00	0.571	0.867
Precision	0.976	0.281	0.414
mAP@.5	0.993	0.479	0.823

achieved a very high performance, with almost perfect recall and precision.

Symbol detection was more difficult. Our symbol detection model achieved an mAP@0.5 of 0.823. The difficulty of this task was not unforeseen, as the symbols are often hand drawn and overlapping, which leads to high variability within a single report (by the same hearing clinician) and from one report to another (between hearing clinicians).

It is the axis label detection model that achieves the lowest performance. While it is true that the font used on the grids varies from one report to another and that this may adversely affect performance, it seems more likely that the scarcity of reports containing label annotations used in training (463) is responsible for this.

### B. Pixel-to-Frequency and Pixel-to-Threshold Transforms Derivation

The most critical step in the algorithm is arguably the accurate derivation of the pixel-to-frequency and pixel-to-threshold transforms. These transforms rely on the accurate detection of at least 2 grid lines and their associated labels per axis. This step is critical, because failure at this step will affect the conversion of *all* symbol coordinates to frequency-threshold pairs downstream. Poor image resolution of the image and the variety of font types used to label the axes make this step the most challenging.

Of the 206 audiology reports used for testing, there were 43 (21%) for which the grid could not be extracted. This occurred when the transforms could not be derived because too few axis labels or grid lines were detected, or because they could not successfully be paired. Two grid reconstructions from the derived transforms are shown in Figure 6: one where the grid was accurately extracted, and one where it was not.

### C. End-to-End Performance of the Digitization Algorithm

To test the end-to-end performance of the digitization algorithm, we ran the complete digitization algorithm on the 206 reports that were not used for training. We computed the precision and recall of the digitization algorithm for every report as follows:

$$Pr = \frac{|\mathcal{T}_{detected} \cap \mathcal{T}_{actual}|}{|\mathcal{T}_{detected}|} \quad (7)$$

$$Sn = \frac{|\mathcal{T}_{detected} \cap \mathcal{T}_{actual}|}{|\mathcal{T}_{actual}|} \quad (8)$$

where  $\mathcal{T}$  is a set of thresholds, each having a symbol (indicating the measurement type, see Table I), a frequency, and a threshold value in decibels.

The digitization algorithm had a mean precision of  $0.66 \pm 0.35$  and a mean recall of  $0.64 \pm 0.35$  over the remaining reports. The distribution of precision and recall is shown in Figure 7A. In total, only 16 reports (7.8%) were digitized perfectly. However, these metrics only capture a small part of the story, as a threshold off by 5 dB is classified incorrect while in many cases, it may not be clinically meaningful. One may wonder why the recall and precision follow each other so closely. This is due to the fact that the algorithm rarely fails to detect a symbol. It is far more common for it to assign an incorrect threshold value to a symbol that actually exists. As a result of the way the precision and recall are computed, if a symbol is given the wrong threshold value, it will be counted

both as a false positive (a threshold that does not exist is predicted) *and* a false negative (actual threshold is missed).

Given that these metrics are strict and do not distinguish between digitized values that are off from the actual value by 5 dB from those that are off by 30 dB, we computed the distribution of distances in dB between the actual and digitized values (Figure 7B). The majority of the incorrectly extracted thresholds (52%) are off by only 5 dB.

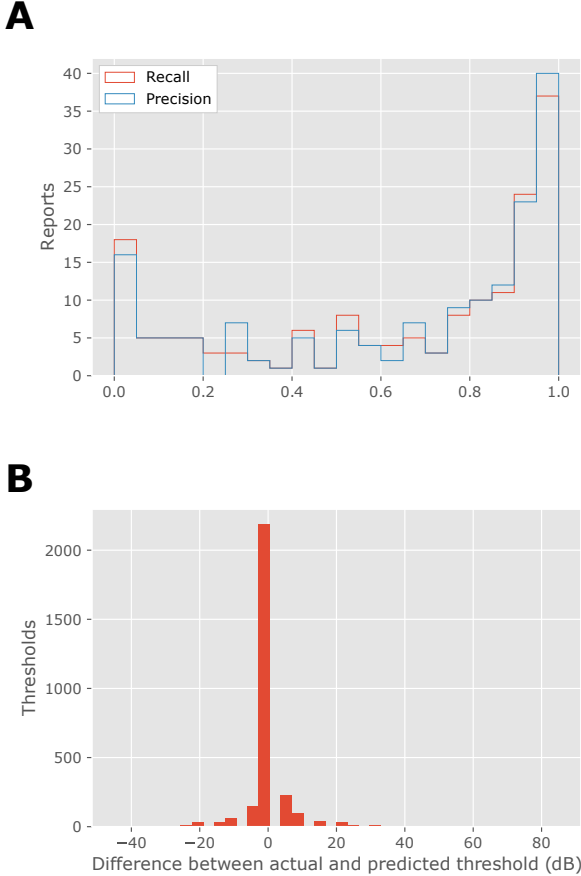


Fig. 7. **Performance of the algorithm in end-to-end digitization.** (A) The recall and precision distribution of the algorithm over 163 successfully digitized reports. (B) The distribution of distances between the actual threshold values and those obtained via digitization.

Factors contributing to the difficulty of the task include the low resolution of the images in our dataset. The fact that the digitization algorithm follows largely a succeed-or-fail trend is mostly caused by a lack of robustness of the grid extraction step which relies on the Hough transform and axis label detection to determine the pixel-to-threshold and pixel-to-frequency transforms. As mentioned previously, failure to properly derive the transforms leads to inaccurate frequencies and/or threshold values for all the detected symbols within a report. Moreover, hearing clinicians are inconsistent in how they report bone conduction thresholds. The widely respected convention for air conduction thresholds is to put the symbol

directly on top of the vertical line indicating a frequency. However, for bone conduction measurements some write down the symbols for the left ear (> and ]) to the right of the frequency line and the symbols for the right ear (< and []) to the left of the frequency line, while others follow the same convention as for air conduction thresholds. Errors in snapping these symbols to the correct frequency adversely affects performance.

## VI. CONCLUSION

In this work, we presented a novel audiogram digitization algorithm capable of extracting hearing thresholds from a variety of handwritten and computer-generated audiology reports as a proof-of-concept. We have shown that even if the task is seemingly simple, the variability in font, resolution, handwriting, and conventions followed by hearing clinicians make the task quite challenging. We believe that the work that is most needed to improve the performance of the algorithm involves refining the grid extraction step to improve its robustness. Collecting additional annotations, especially for axis labels, to retrain the axis label detector could also significantly improve the performance of the algorithm. At this time, the algorithm lacks the accuracy to be deployed in an unsupervised fashion, but combined with human supervision and corrections, it can still drastically speed up the digitization process by requiring only some manual adjustments to the extracted thresholds. The NIHL portal bootstraps the audiogram digitization algorithm to produce an initial annotation that can rapidly be adjusted by the annotator. This allows for the expansion of the dataset to further train the audiogram, axis labels, and symbol detection deep neural networks to enhance their accuracy.

We anticipate that this work will be of great interest not only to insurance companies, who must process scanned or faxed audiological reports, but will also be useful to researchers in the field of audiology interested in using archived audiological records in paper format and to hospitals and clinics in migrating records in their archives to a digital format.

## ACKNOWLEDGMENT

The authors would like to thank Sherine Stephens, Valerie Hilton, Eric Gordon and Ian Cross from the WSIB Innovation Labs for providing the data that was used in this work. Furthermore, the authors also thank Jaser El-Habrouk, Abhinav Yalamanchili, Ahmed Abdelrazik, Jason Fernandes, Tanzin Norjin, Syed Ahmed, Kenneth Calangan, Brandon Ca and Vivian Han who each contributed numerous hours to annotate hundreds of audiological reports.

## REFERENCES

- [1] K. Feder, D. Michaud, J. McNamee, E. Fitzpatrick, H. Davies, and T. Leroux, "Prevalence of Hazardous Occupational Noise Exposure, Hearing Loss, and Hearing Protection Usage Among a Representative Sample of Working Canadians," *Journal of Occupational and Environmental Medicine*, vol. 59, no. 1, pp. 92–113, Jan. 2017. [Online]. Available: <http://journals.lww.com/00043764-201701000-00015>
- [2] P. M. Rabinowitz, "Noise-induced hearing loss," *American Family Physician*, vol. 61, no. 9, pp. 2749–2756, May 2000. [Online]. Available: <https://www.aafp.org/afp/2000/0501/p2749.html>

- [3] Ultralytics, “YOLOv5,” 2020. [Online]. Available: <https://github.com/ultralytics/yolov5>
- [4] T.-Y. Lin, M. Maire, S. Belongie, L. Bourdev, R. Girshick, J. Hays, P. Perona, D. Ramanan, C. L. Zitnick, and P. Dollár, “Microsoft COCO: Common Objects in Context,” *arXiv:1405.0312 [cs]*, Feb. 2015, arXiv: 1405.0312. [Online]. Available: <http://arxiv.org/abs/1405.0312>
- [5] H. Rezatofighi, N. Tsoi, J. Gwak, A. Sadeghian, I. Reid, and S. Savarese, “Generalized Intersection Over Union: A Metric and a Loss for Bounding Box Regression,” in *2019 IEEE/CVF Conference on Computer Vision and Pattern Recognition (CVPR)*. Long Beach, CA, USA: IEEE, Jun. 2019, pp. 658–666. [Online]. Available: <https://ieeexplore.ieee.org/document/8953982/>
- [6] R. O. Duda and P. E. Hart, “Use of the Hough transformation to detect lines and curves in pictures,” *Communications of the ACM*, vol. 15, no. 1, pp. 11–15, Jan. 1972. [Online]. Available: <https://doi.org/10.1145/361237.361242>
- [7] Google, “tesseract-ocr/tesseract,” Nov. 2020, original-date: 2014-08-12T18:04:59Z. [Online]. Available: <https://github.com/tesseract-ocr/tesseract>